A&A 480, 305–312 (2008)
DOI: 10.1051/0004-6361:20079085

Astronomy & Astrophysics

Prompt GRB emission from gradual energy dissipation

D. Giannios

Max Planck Institute for Astrophysics, Box 1317, 85741 Garching, Germany
e-mail: giannios@mpa-garching.mpg.de

Received 16 November 2007 / Accepted 24 December 2007

ABSTRACT

I calculate the emission expected from a Poynting-flux-dominated gamma-ray burst (GRB) flow in which energy is dissipated gradually by magnetic reconnection. In this picture, the energy of the radiating particles is determined by heating and cooling balance (slow heating model). Detailed radiative transfer calculations show that, at Thomson optical depths of order of unity, the dominant radiative process is inverse Compton scattering. Synchrotron-self-absorbed emission and inverse Compton dominate in the Thomson thin parts of the flow. The electrons stay thermal throughout the dissipation region because of Coulomb collisions (Thomson thick part of the flow) and exchange of synchrotron photons (Thomson thin part). The resulting spectrum naturally explains the observed sub-MeV break of the GRB emission and the spectral slopes above and below the break. The model predicts that the γ-ray power-law tail has a high-energy cutoff typically in the $\sim$0.1−1 GeV energy range that should be observable with *GLAST*. The model also predicts a prompt emission component in the optical and UV associated with the GeV emission. Observations of the prompt emission of GRB 061121 that cover the energy range from the optical to $\sim$1 MeV are explained by the model.

Key words. gamma rays: bursts – radiation mechanisms: general – methods: statistical

1. Introduction

The GRB emission is the likely result of internal energy release in an ultrarelativistic flow. The dissipative and radiative mechanisms for the GRB largely remain uncertain. A popular model for the energy dissipation invokes internal shocks in an unsteady flow (Paczynski & Xu 1994; Rees & Mészáros 1994). An alternative proposal is magnetic dissipation in a strongly magnetized flow (Thompson 1994; Spruit et al. 2001)

Internal shocks are efficient in dissipating a large fraction of the kinetic energy of the flow provided that it is highly variable, i.e., composed of distinct ejection events with strong variation in their bulk Lorentz factor γ (e.g. Kobayashi et al. 1997). Energy is dissipated by the shocks at the location of the collision of the shells. Particles are assumed to be accelerated on a very short timescale at the shock front to ultrarelativistic speeds and non-thermal distributions. Subsequently, they radiate a fraction of the dissipated energy via synchrotron and inverse Compton processes. The relevant radiative mechanisms and the emitted spectra depend, to a large extent, on the shock microphysics and the corresponding Thomson optical depth of the flow at the radius of the collision (see, e.g., Pe'er et al. 2006)

On the other hand, the energy dissipation that powers the GRB emission may be gradual and distributed over a large part of the volume of the flow. The energy of the radiating particles is determined by the heating/cooling equilibrium (slow heating model; Ghisellini & Celotti 1999; Stern & Poutanen 2004). Such an energy balance is expected to lead to sub-relativistic or mildly relativistic temperatures in the flow. Magnetic dissipation in a strongly magnetized flow can provide a possible physical setup where gradual dissipation is realized. As shown in Drenkhahn (2002) and Drenkhahn & Spruit (2002, hereafter DS02), dissipation though reconnection takes place over several decades in radius, typically in both Thomson thick and thin conditions. Dissipation in the reconnection model is responsible for both the acceleration of the flow and the prompt emission.

1.1. Emission from magnetic dissipation

In previous works (Giannios 2006; Giannios & Spruit 2007, hereafter G06 and GS07 respectively), we studied the radiative transfer close to the Thomson photosphere of the flow in the context of the magnetic reconnection model. The detailed Monte Carlo calculations have shown that, due to energy release, the flow develops a hot photosphere with comoving electron temperatures of tens of keV. In the photospheric region, Coulomb collisions are fast enough to thermalize the electron distribution. Upscattering of photons that are produced deeper in the flow by those hot electrons leads to a powerful photospheric emission; it accounts for $\sim$3−30% of the luminosity of the flow. The resulting $E \cdot f(E)$ spectrum has a characteristic $\sim$1 MeV peak followed by a flat high-energy power-law emission.

Here, I extend the radiative transfer calculation to the Thomson thin region of the flow where, in the reconnection model, there can be substantial energy release and associated emission. Because of the strong magnetic fields, synchrotron self absorption results in efficient energy exchange of the electrons, keeping their distribution thermal (Ghisellini et al. 1998). I show that heating and cooling balance in that region leads to electron temperatures of the order of the electron rest mass. Under these conditions, synchrotron-self-absorbed (SSA) emission is an important radiative mechanism in addition to inverse Compton. SSA dominates the observed emission in the soft X-rays and softer bands.

The efficient thermalization of the emitting particles throughout the flow reduces the dependence of the model on the, poorly understood, mechanisms of particle acceleration

that operate in magnetic reconnection. The model is defined by just 3 main parameters (luminosity, baryon loading and a reconnection-rate parameter; see Sect. 3). In contrast to the internal shock model, no quantities have to be added to parameterize the particle distributions and the amplification of magnetic fields; the field strength is an integral part of the reconnection model. Because the model is so well defined, it makes direct and stable predictions for the emitted spectrum. In the following, I show how this spectrum can be computed.

The structure of the paper is the following. In the next section I summarize and contrast the main aspects of internal shock and magnetic reconnection models for the prompt GRB emission. The dynamics of the flow in the reconnection model and the radiative transfer in the flow are the topic of Sects. 3 and 4 respectively. The resulting spectra and their direct comparison with multi-frequency observations (from optical to γ-rays; see Page et al. 2007) of GRB 061121 are presented in Sect. 5. I discuss the results and conclude in Sect. 6.

2. Magnetic reconnection versus internal shocks

The internal shock model for the GRB emission invokes high variability in the bulk Lorentz factor of the flow that leads to internal collisions. The location where the collision of two shells takes place depends on their initial separation and bulk Lorentz factors. These collisions can dissipate a substantial fraction of the kinetic energy of the flow. Internal shocks are assumed to lead to particle acceleration and magnetic field amplification at the shock front. If electrons receive a large fraction of the dissipated energy then they are accelerated to ultrarelativistic speeds. They cool down radiatively by synchrotron and inverse Compton mechanisms. The resulting spectrum and the relevant radiative mechanisms depend on details of the distribution of the accelerated particles, the magnetic field strength and the Thomson optical depth of the flow at the location of the collision. If the collision of two shells takes place at the Thomson thin region, as needed to explain the typical variability properties of the GRB lightcurves (Daigne & Mochkovitch 1998; Nakar & Piran 2002; Mimica et al. 2005), synchrotron self Compton is likely the most promising radiative mechanism (Rees & Mészáros 1994; Katz 1994; Tavani 1996). In this picture optically thin synchrotron emission dominates the observed hard X-ray, ~MeV spectrum. Despite its attractive features, the synchrotron model has theoretical and observational difficulties (as discussed, for example, in Ghirlanda et al. 2003). If, on the other hand, the collisions take place close to the Thomson photosphere, Compton scattering is the dominant radiative mechanism that shapes the spectrum and results in very different emission (Pe'er et al. 2006).

As an alternative to internal shocks, magnetic dissipation can power the prompt emission provided that the flow is launched Poynting-flux dominated (or with a substantial fraction of its energy in the form of Poynting flux). Magnetic dissipation through, for example, reconnection can release energy smoothly in a large fraction of the volume of the flow. This energy release can take place while the flow expands over several decades in radius (DS02). The energy of the radiating particles is determined by balancing heating and radiative (or adiabatic) cooling at each radius. In this case the slow heating picture described by Ghisellini & Celotti (1999) takes place. The electrons are subrelativistic or mildly relativistic and their synchrotron emission is self absorbed. In a strongly magnetized flow, such SSA emission guarantees efficient energy exchange and thermalization of the electrons on a very short timescale (Ghisellini et al. 1998). The resulting emission does not depend on details of particle acceleration and magnetic field amplification that one faces in internal shock models. The model is defined by just the luminosity, the baryon loading and the reconnection-rate parameter of the flow. This contributes significantly to the predictive power of the magnetic reconnection model. The total observed flux is the integrated emission from the different parts of the flow in which dissipation of energy takes place. It contains both photospheric (Thompson 1994; Stern 1999; G06; GS07) and Thomson thin components (this work).

2.1. Implications from the observed GRB variablity

One additional difference of the internal shock and the magnetic reconnection model is connected to implications from the observed variability of the lightcurves. Internal shocks are efficient only in variable flows. Variability and dissipation are, a priori, unrelated in the magnetic reconnection model in which dissipation takes place, even in a steady outflow. On the other hand, the observed lightcurves are often highly variable showing that the flow does evidently evolve during a GRB. In the context of the reconnection model, the observed variability reflects changes in the luminosity and baryon loading of the flow during the burst. As shown in GS07, the flow can be treated as quasi-stationary for all but the shortest time scales observed in a burst, the variation of spectral properties during a burst directly reflects variations in the central engine. This is in contrast to models in which the prompt radiation is produced at much larger distances from the source, such as external shock models. It is also in contrast with the internal shock model, since the internal evolution of the flow between the source and the level where radiation is emitted is a key ingredient in this model. Deducing properties of the central engine from observed burst properties is thus a much more direct prospect in the magnetic dissipation model.

3. Gradual energy release because of magnetic reconnection

Magnetic dissipation can take place gradually in the GRB flow. The rate at which energy is dissipated as a function of radius depends on the magnetic field geometry and the exact mechanism through which magnetic energy dissipates. If the flow is launched with field of large scale, energy dissipation can be a result of global MHD instabilities (such as current-driven instabilities; e.g., Lyutikov & Blandford 2003; Giannios & Spruit 2006). On the other hand, if the flow contains reversing magnetic fields of sufficiently small scale, dissipation can take place directly through reconnection (Drenkhahn 2002; DS02; Thompson 2006). Here, I focus on the reconnection model, which makes clear prediction for the energy dissipation as a function of radius; essential for the radiative transfer calculations presented here. Though the results presented here are directly applicable to the DS02 model, qualitatively similar results are expected from other gradual, magnetic dissipation models.

3.1. The reconnection model

An important physical quantity in the reconnection model is the ratio σ_0 of the Poynting flux to kinetic energy flux at the Alfvén radius r_0. This quantity parameterizes the baryon loading of the flow η and determines the terminal bulk Lorentz factor of the flow $\gamma_\infty \sim \eta \simeq \sigma_0^{3/2}$. The flow must start Poynting-flux

dominated with $\sigma_0 \gtrsim 30$ for it to be accelerated to ultrarelativistic speeds with $\gamma_\infty \gtrsim 100$ that are relevant for GRB flows.

In the reconnection model, the magnetic field in the flow changes polarity on a scale λ. If the magnetic field anchored in the rotating central engine is nonaxisymmetric, this scale is (in the central engine frame) of the order of the light cylinder r_l: $\lambda \simeq 2\pi c/\Omega$, where Ω is the angular frequency of the rotator. This is as in the oblique rotator model for pulsar winds (Coroniti 1990). This model has been further developed to include special relativistic effects and different reconnection prescriptions (Lyubarsky & Kirk 2001; DS02; Kirk & Skjæraasen 2003). The rate of magnetic reconnection DS02 model is parameterized through the velocity v_r with which magnetic fields of opposite direction merge. The v_r is assumed to scale with the Alfvén speed, v_A, i.e. $v_r = \varepsilon v_A$. A nominal value used for ϵ is 0.1 (see Lyubarsky 2005). For the flows with $\sigma_0 \gg 1$ that are of interest here, the energy density of the magnetic field is larger than the rest mass energy density, hence $v_A \approx c$, and the reconnection takes place with subrelativistic speeds.

3.1.1. Properties of the flow

In the reconnection model, magnetic dissipation takes place all the way from the initial radius r_0 till the saturation radius r_s. Part of the dissipated energy (approximately half) is directly used to accelerate the flow. The acceleration of the flow is gradual following the $\gamma \sim r^{1/3}$ scaling as function of radius in the regime $r_0 \ll r \ll r_s$. To first order approximation, no further acceleration takes place beyond the saturation radius. Summarizing the results derived in Drenkhahn (2002), the bulk Lorentz factor of the flow is approximately given by

$$\gamma = \gamma_\infty \left(\frac{r}{r_s}\right)^{1/3} = 148\, r_{11}^{1/3} (\varepsilon\Omega)_3^{1/3} \sigma_{0,2}^{1/2}, \quad \text{for} \quad r < r_s,$$
$$\gamma = \gamma_\infty = \sigma_0^{3/2}, \quad \text{for} \quad r \geq r_s, \tag{1}$$

while the saturation radius is

$$r_s = \frac{\pi c \gamma_\infty^2}{3\varepsilon\Omega}; \quad \text{or} \quad r_{s,11} = 310\, \frac{\sigma_{0,2}^3}{(\varepsilon\Omega)_3}\,. \tag{2}$$

The notation $A = 10^x A_x$ is used; the "reference values" of the model parameters are $\sigma_0 = 100$, $\varepsilon = 0.1$, $\Omega = 10^4$ rad s^{-1}. The product of ε and Ω parameterizes the reconnection rate. The physical quantities of the flow depend on this product.

In the steady, spherical flow under consideration the comoving number density can be written as

$$n' = \frac{L}{r^2 \sigma_0^{3/2} \gamma m_p c^3}, \tag{3}$$

where L is the luminosity per steradian of the GRB flow. The reference value used is $L = 10^{52}$ erg s^{-1} sterad^{-1}. (In this form the expression can be compared with the fireball model, where the baryon loading parameter η replaces the factor $\sigma_0^{3/2}$.)

The expression (1) is deviating from the exact numerical solution presented in Drenkhahn (2002) at $r \gtrsim r_s$. The reason is that the dissipation does not stop abruptly at r_s but there is modest energy release at a slower rate at larger radii. This leads to modest acceleration of the flow at $r \gtrsim r_s$. In the following, we ignore these deviations and use the expressions (1) and (3) for the bulk Lorentz factor and density of the flow respectively. This simplification facilitates the radiative transfer study in the flow.

On the other hand, quantities of the flow such as magnetic field strength and the energy dissipation rate as functions of radius need to be followed in more detail around r_s. Though, not important for the global energetics, the remaining dissipation at the radii $r \gtrsim r_s$ results in synchrotron emission that dominates the observed radiation in soft bands (such as optical and near ultra violet). This emission is mainly a result of the large emitting surface at these outer parts of the flow. I take into account the residual dissipation to correctly describe the soft emission. In the calculations that follow I calculate the magnetic field strength and dissipation rate by solving the relevant differential equations that describe the full 1D relativistic MHD problem as presented in Drenkhahn (2002, summarized by Eq. (38) in that paper). Still, for the purpose of estimates, I give analytic expressions for these quantities that are accurate below the saturation radius.

The comoving magnetic field strength B' below the saturation radius is given by setting $L \simeq L_p = r^2 B'^2 \gamma^2 c/4\pi$ and solving for B':

$$B' = \left(\frac{4\pi L}{c r^2 \gamma^2}\right)^{1/2} \quad \text{for} \quad r < r_s. \tag{4}$$

The rate of energy density release in a comoving frame can be found by the following considerations. The time scale over which the magnetic field decays is that of advection of magnetic field of opposite polarity to the reconnection area. The reconnection speed is $v_r = \varepsilon v_A \simeq \varepsilon c$, while the magnetic field changes polarity over a comoving length scale $\lambda' = 2\pi\gamma c/\Omega$. The decay timescale for the magnetic field, therefore, is

$$t_{dec} = \frac{\lambda'}{v_r} = \frac{2\pi\gamma}{\varepsilon\Omega}\,. \tag{5}$$

Using the last expression and Eqs. (1) and (4), the rate of dissipation of magnetic energy density in the comoving frame is

$$P_{diss} = \frac{(B')^2/8\pi}{t_{dec}/2} = \frac{\varepsilon\Omega L}{2\pi c r^2 \gamma^3} \quad \text{for} \quad r < r_s. \tag{6}$$

The bulk Lorentz factor γ, the density n', the magnetic field strength B' and rate of dissipation of magnetic energy density P_{diss} of the flow as functions of radius are the quantities needed for the study of the resulting emission.

4. Photospheric and Thomson thin emission

If all the energy is dissipated deeply into the GRB flow (i.e. at large optical depths), adiabatic expansion converts most of this energy into kinetic at the expense of radiation. Gradual dissipation heats the flow continuously and maintains a substantial fraction of the energy in the form of radiation. This radiation is released at the photosphere of the flow. If dissipation takes place further out in the flow it can result in additional emission coming from the Thomson thin region. The total flux received by the observer is the integrated emission from the different parts of the flow where dissipation takes place.

In the case of magnetic dissipation (as well as for other dissipative mechanisms), the fate of the released energy is rather uncertain. An interesting possibility is that dissipation leads to MHD turbulence where particle acceleration can take place by scattering of photons by Alfvén waves (Thompson 1994). On the other hand, the magnetic energy can directly be dissipated to the particles in the flow, most likely to the electrons due to their higher mobility. Following G06, GS07 we assume that a

fraction f_e of order of unity of the dissipated energy heats up the electrons. For the results presented here we set $f_e = 0.5$.

The resulting emission does not depend only on the amounts of energy released but also on the distribution of the emitting particles. I assume that the electron distribution is thermal *throughout* the region where dissipation takes place. As I discuss in more detail in Sect. 4.2.1, the thermalization of the electrons is result of Coulomb collisions in the inner parts of the flow and of exchange of synchrotron photons at the outer parts. I first summarize the results of G06, GS07 on the photospheric emission from the reconnection model and then turn to the study of the Thomson thin emission.

4.1. Photospheric emission

In addition to the saturation radius r_s, another characteristic radius of the flow is the Thomson photosphere. The Thomson optical depth as a function of radius is $\tau \sim n'\sigma_T r/\gamma$. It can be expressed in terms of the parameters of the flow (e.g. G06):

$$\tau = \frac{20}{r_{11}^{5/3}} \frac{L_{52}}{(\varepsilon\Omega)_3^{2/3}\sigma_{0,2}^{5/2}}. \quad (7)$$

As expected, at small radii to optical depth is large and vice-versa. The radius of the Thomson thick-thin transition is found by setting $\tau = 1$ in Eq. (7) and solving for r_{ph}:

$$r_{ph,11} = 6\frac{L_{52}^{3/5}}{(\varepsilon\Omega)_3^{2/5}\sigma_{0,2}^{3/2}}. \quad (8)$$

In deriving these expressions, we have assumed that $r_{ph} < r_s$. A similar calculation gives the radius of the photosphere in the $r_{ph} > r_s$ case.

One can check that for a large parameter space relevant for GRB flows, $r_{ph} < r_s$ which means that dissipation proceeds throughout the photospheric region. In terms of the physical properties of the flow, there is a critical value of the magnetization $\sigma_{0,cr}$, for which $r_{ph} = r_s$. For $\sigma_0 > \sigma_{0,cr}$, $r_{ph} < r_s$. Using Eqs. (8) and (2) one finds

$$\sigma_{0,cr} = 42\left(L_{52}(\varepsilon\Omega)_3\right)^{2/15}. \quad (9)$$

The critical baryon loading depends weakly on the parameters of the flow: $\eta_{cr} = \sigma_{0,cr}^{3/2} = 270\left(L_{52}(\varepsilon\Omega)_3\right)^{1/5}$.

For $\sigma_0 \ll \sigma_{0,cr}$ dissipation ceases deep in the flow (at high optical depths). For $\sigma_0 \gg \sigma_{0,cr}$, dissipation takes place in both Thomson thick and thin conditions with most of the energy released in the outer parts of the flow. The implications of such energy release to the properties of the flow and the resulting radiation have been studied in G06 and GS07. Those studies focused on the Thomson thick part of the flow and the photospheric region out to $\tau \sim 0.1$. Observational effects from Thomson thin dissipation were not considered in detail and are the topic of this paper.

The main results of the G06, GS07 papers are the following. Particles and radiation are found to be in thermal equilibrium deep in the flow. There, the comoving temperature T_{th} of the flow is calculated, under the assumption of complete thermalization, by integrating the energy released at different radii in the flow and taking into account adiabatic cooling. Due to the dominance of scattering, the details of radiative transfer become important already at fairly large optical depth in the flow. Equilibrium between radiation and matter holds only at Thomson depths greater than about 50. At smaller optical depths the electron distribution stays thermalized, but is out of equilibrium with the photon field. More discussion on the processes that lead to thermalization of the electron distribution is presented in the next section. Compton scattering of the photons is treated in detail in this region with Monte Carlo Comptonization simulations (G06; GS07). Energy dissipation at moderate and low optical depths is shown to lead to emission that has a highly non-thermal appearance.

For $\sigma_0 \gtrsim \sigma_{0,cr}$, the flow develops a hot photospheric region. The electron temperature at moderate optical depths can be estimated analytically by balancing the heating (Eq. (6)) with the inverse Compton cooling rate $P_{Comp} = 4k_B T_e n' c\sigma_T u_r/m_e c^2$, where u_r is the energy density of radiation. The electron temperature can be expressed as a function of optical depth in the flow (the detailed numerical results verify these estimates; see G06):

$$T_e \simeq \frac{40 f_e}{\tau}\,\mathrm{keV}, \quad \text{for} \quad 0.1 \lesssim \tau \lesssim 50. \quad (10)$$

For $\tau \gtrsim 50$, the electron temperature equals that of the photon field. For $\tau \lesssim 0.1$, the electrons become mildly relativistic and one has to consider relativistic corrections to the Compton cooling to derive the appropriate expression for the temperature. At these larger radii (or lower τ) the electron temperature becomes high enough that synchrotron emission (and associated cooling of the particles) has to be taken into account.

4.2. Emission from the Thomson thin region

Magnetic dissipation around the Thomson photosphere leads to subrelativistic electrons that are more energetic with respect to the average photon in the flow. Under these conditions the dominant mechanism that shapes the spectrum is inverse Compton scattering. Synchrotron emission is negligible since it is strongly self absorbed. When dissipation continues at the optically thin parts of the flow the electron temperature becomes of the order of the electron rest mass. At those temperatures, synchrotron self Compton emission has important effect on the emitted spectrum (see also Stern & Poutanen 2004). Furthermore, SSA affects the electron distribution in the flow.

4.2.1. Thermalization of the electrons

At high optical depths, the density of the flow is high and the electron temperature rather low (see Eq. (10)). Under these conditions, Coulomb collisions are efficient in thermalizing the electron distribution. This is not the case in the Thomson thin parts of the flow (G06). On the other hand, there is a more efficient channel for energy exchange among electrons. It is shown in Ghisellini et al. (1998) that electrons with energy of the order of their rest mass can thermalize on a few synchrotron cooling times (as defined for thin synchrotron emission) by emitting and absorbing synchrotron photons. In the magnetically dominated flow under consideration, the thermalization of the electrons takes place on a timescale shorter than the heating/cooling one. One can, therefore, assume that the electrons are approximately thermal when calculating their emission.

A caveat in the previous argument is connected to the underlying assumption that the dissipated energy is distributed to a large fraction of the particles in the flow. If the magnetic reconnection leads, for example, to deposition of most of the energy to a small fraction of the electrons, they can be accelerated to relativistic speeds and cool efficiently through thin synchrotron

emission. In this case, synchrotron self absorption is not an efficient thermalization mechanism. This case has been investigated in Giannios & Spruit (2005). From this point on we assume that the dissipated energy is distributed among a large fraction of the particles and hence thermalization is achieved in the electron distribution.

4.2.2. Modeling of the synchrotron emission

The electron temperature becomes mildly relativistic at small optical depths $\tau \sim 0.1$ (see Eq. (10)). It increases further at larger radii resulting in substantial synchrotron emission. The synchrotron-self-absorbed emission from mildly relativistic plasma has a characteristic spectrum that consists by a Rayleigh-Jeans part up to the so-called turnover frequency ν_t where the optical depth due to synchrotron absorption of the flow becomes unity. Most of the energy is emitted at the turnover frequency. At higher frequencies, the spectrum is very steep following the exponentially decaying tail of the synchrotron thin emission. The energy density per unit frequency of the synchrotron photons in a frame comoving with the flow is $u_\nu = 8\pi\nu^2 k_B T/c^3$ for $\nu \le \nu_t$, while it drops very fast for $\nu > \nu_t$. The energy density of the synchrotron photons is given by integrating the last expression: $u_s = \int u_\nu d\nu \simeq 8\pi\nu_t^3 k_B T/3c^3$. The synchrotron luminosity per steradian at radius r is:

$$L_s = \frac{4r^2\gamma^2 u_s c}{3} \simeq \frac{32\pi r^2\gamma^2\nu_t^3 k_B T_e}{9c^2}\,. \tag{11}$$

The synchrotron emission depends strongly on the turnover frequency. The turnover frequency can be related to the magnetic field strength B', the electron temperature T_e and the Thomson optical depth τ of the flow. For the mildly relativistic plasma under consideration the calculation of the synchrotron emission and the corresponding absorption is rather evolved. On the other hand, there are studies focusing on developing approximate expressions for the synchrotron emission (and therefore absorption) at this temperature regime (e.g. Petrosian 1981; Mahadevan & Narayan 1996; Zdziarski et al. 1998; Wardziński & Zdziarski 2000). Here I use the approximate analytic expressions for ν_t derived in Zdziarski et al. (1998):

$$\nu_t = \frac{343}{36}\theta_e^2\nu_c \ln^3\frac{C}{\ln\frac{C}{\cdots}}, \tag{12}$$

where $\nu_c = eB'/2\pi m_e c$ is the cyclotron frequency and $\theta_e = k_B T_e/m_e c^2$. The quantity C is defined as[1]

$$C = \frac{3}{7\theta_e}\left[\frac{\pi m_e c^2\tau e^{1/\theta_e}}{3\alpha_f h\nu_c}\right]^{2/7}, \tag{13}$$

where h, α_f are Planck's and fine structure constants respectively. For typical model parameters and radii $r \sim r_s$, the turnover frequency is $\nu_t \sim 10^3\nu_c$ which results in $\nu_t^{obs} = \gamma_\infty\nu_t/(1+z) \lesssim 1$ keV (z is the redshift of the burst). The synchrotron-self-absorbed emission appears mainly in the soft X-rays and softer bands.

The expression (12) has been compared with the exact numerical results and shown to be overestimating the turnover frequency (and consequently the synchrotron emission) in plasma with $\theta_e \lesssim 0.1$ (see Fig. 2b in Wardziński & Zdziarski 2000). On the other hand, it is quite accurate for higher electron temperatures. Since most of the synchrotron emission comes from regions of the flow with $\theta_e \sim 1$, Eq. (12) is accurate enough for the calculations presented here.

One can now extend the Comptonization calculation developed in G06 to include the radiative transfer in the Thomson thin region of the flow. The procedure is the following. I make a choice for the temperature profile as a function of radius of the electron temperature in the flow. Analytical expressions such as that of Eq. (10) provide a good initial guess. The radiative transfer in the flow is studied using the Monte Carlo Comptonization code described in G06. The calculation includes the thermal radiation field carried with the flow which is injected in the inner numerical boundary at the "equilibrium" radius where radiation and particles drop out of equilibrium. At larger radii the synchrotron emitted flux is also included (using expressions (11), (12)). Both sources of photons are propagated through the medium and their scattering by electrons is followed. The code calculates the spectrum and the radius-dependent cooling rate of the electrons. Cooling because of inverse Compton, synchrotron emission and adiabatic expansion is taken into account. The adiabatic cooling becomes important at high optical depths and at the very outer parts of the flow where the expansion timescale $r/\gamma c$ is shorter than the radiative cooling one. The outer boundary of the calculations is set at large enough radius so that it does not have an effect on the computed spectra. I iterate the electron temperature until the cooling rate matches the heating rate predicted by the model reasonably well at all radii. In practice, I make sure that they match within ~30% or less everywhere. Considering the rather larger uncertainties in the model coming from, for example, the assumed dynamics of the flow, this a fairly accurate calculation.

5. Resulting spectra

First, I focus on the new features that appear in the emitted spectrum w.r.t. the G06 results because of the inclusion of the Thomson thin emission. In the illustrative case of Fig. 1, I set $\sigma_0 = 70$ (which corresponds to flow with baryon loading $\eta \simeq \sigma_0^{3/2} \sim 600$) and the rest of the parameters to their reference values. Spectra are plotted in the central engine frame. The dotted line shows the input thermal radiation at the "equilibrium radius" which is the inner boundary of the computed domain. The thermal flux is advected with the flow and constitutes a large fraction of the seed photons to be Comptonized further out in the flow.

The appearance of the photon spectrum at radius which corresponds to optical depth $\tau = 0.1$ is shown with dashed line. This radius is the outer boundary used in most of the calculations of G06, GS07. One can clearly see the effect of inverse Compton scattering to the spectrum. The peak of the $E \cdot f(E)$ spectrum increases slightly and the spectrum becomes broader. An important feature is the high-energy tail that is the result of unsaturated Comptonization at $\tau \lesssim 1$. Note also a second peak at ~1 keV. This is the result of synchrotron emission with the turnover frequency being ~1 keV (in the central engine frame). This component is still weak at $\tau = 0.1$ and has not been included in the calculations of G06, GS07.

The total spectrum is shown with solid line. This includes the emission from the whole volume of the flow where dissipation takes place. The overall emission spectrum is much broader. It is characterized by a break at ~1 MeV followed by a flat spectrum with photon-number index $\Gamma \simeq -2$ (where $dN/dE \sim E^\Gamma$), close to the typically observed one. The hard γ-ray tail is extending up to ~1 GeV which corresponds to the Lorentz boosted temperature of the flow at its outer layers (where it reaches its maximum

[1] Here I set the Zdziarski et al. (1998) correction factor $A_M = 1$.

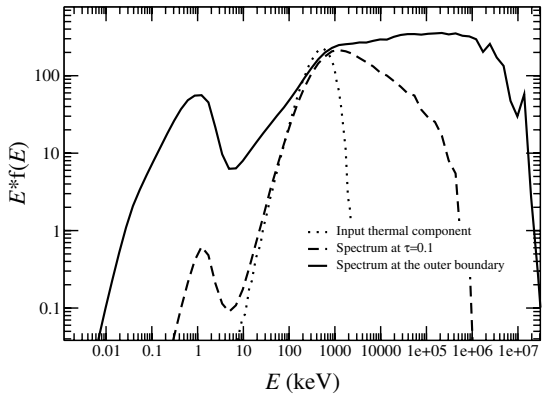

Fig. 1. Photon spectrum at different radii (or corresponding Thomson optical depths) in the flow. The spectrum is shown in the central engine frame. The dotted line stands for the spectrum at the radius where radiation and electrons decouple. The photospheric emission is shown with the dashed line (see also G06; GS07). The overall spectrum (solid line) includes the emission from the Thomson thin region of the flow. Synchrotron-self-absorbed emission from this region dominates the spectrum below ∼10 keV. Inverse Compton leads to flat γ-ray tail up to ∼1 GeV.

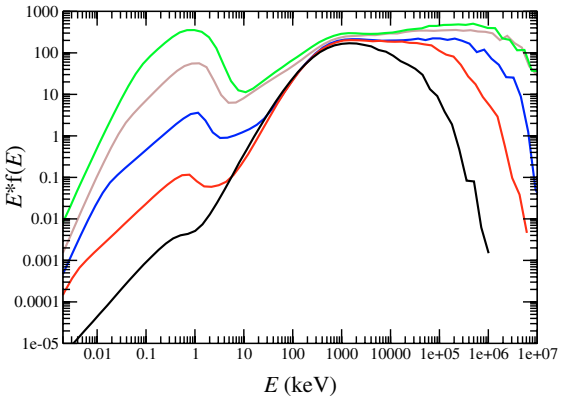

Fig. 2. Resulting spectrum (in the central engine frame) for different baryon loadings of the flow. From bottom to top the curves correspond to magnetization $\sigma_0 = 40, 50, 60, 70, 100$ (or corresponding baryon loading $\eta \simeq 250, 350, 460, 590, 1000$) respectively. The high σ_0 flows are characterized broader spectra. The model predicts that bright prompt optical and UV emission is accompanied by powerful ∼GeV emission. For bright optical emission, the optical spectrum is expected to be hard.

values). Comparing the spectrum at $\tau = 0.1$ and the total one, it is clear that Comptonization proceeds throughout the Thomson thin region strengthening the hard γ-ray component.

An important new feature is the powerful emission that appears in the soft X-rays and softer bands. This comes from synchrotron-self-absorbed emission. SSA dominates by many orders of magnitude the ultra violet and optical emission. The softer emission originates from the Thomson thin part of the flow that is characterized by the higher electron temperatures and larger emitting surface (see also Stern & Poutanen 2004). This emission is very weak in models where dissipation takes place below or around the Thomson photospheric region (see, e.g., Mészáros & Rees 2000; Pe'er et al. 2006; Ioka et al. 2007).

As a result of the synchrotron-self-Compton component, the spectrum below the MeV peak softens with respect to the G06 calculation where only the photospheric component was considered. The spectrum can be well fitted with a power-law in the 30−300 keV energy range with photon-number index of $\Gamma \simeq -1.2$ which very close to the one typically observed (e.g. Preece et al. 1998).

In this example, the SSA emission spectrum hardens considerably below ∼30 eV. At lower energies the Rayleigh-Jeans limit is gradually approached. The location of the hardening is determined by the radius where adiabatic expansion starts to dominate the cooling of the electrons. In this example adiabatic expansion dominates at $r \gtrsim r_{\rm ad} \sim 5 \times 10^{14}$ cm. Most of the radiation observed at $E \lesssim 30$ eV comes from this radius. The optical and near UV emission is delayed w.r.t. the ∼MeV emission by $\delta t \sim r_{\rm ad}/\gamma_\infty^2 c \sim 0.05$ s. Radiation in these bands reaches the observer with small but maybe detectable lags. In the region $30 \lesssim E \lesssim 1000$ eV the spectral slope depends on the radial dependence of the turnover frequency $\nu_{\rm t}$.

The relative strength of the synchrotron-self-Compton (SSC) component depends on the fraction of energy dissipated in the Thomson thin region of the flow. For $\sigma_0 \gg \sigma_{0,\rm cr}$ most of the energy is dissipated in the Thomson thin region. Correspondingly the SSC component is pronounced. This is evident in Fig. 2 where the spectrum is shown for different values of σ_0 (the rest of the parameters are kept in their reference values). For $\sigma_0 = 40$, dissipation stops close to the photosphere of the flow. The SSA component is almost absent and the emission above the thermal peak at ∼1 MeV relatively weak. In more baryon loaded models the emission is quasi-thermal since dissipation stops at high Thomson depths.

With increasing σ_0 both the SSA and inverse Compton components become relatively more powerful. The thermal peak is followed by a flat γ-ray emission that extends up to ∼0.1−1 GeV. Most of the models show a high energy cutoff in this energy range. This cutoff corresponds to the highest energies to which photons are upscattered. It is determined by the Lorentz boosted electron temperature at $r \sim r_{\rm s}$. The spectral slope below the ∼1 MeV break becomes softer with increasing σ_0. The photon-number index in the 30−300 keV energy band varies in the range $-1.2 \lesssim \Gamma \lesssim -0.4$ in agreement to that typically observed (e.g. Preece et al. 1998). The high σ_0 models have powerful optical and near ultra violet emission. The flux $f(E)$ that is emitted in these bands is similar to the X-rays one. The optical spectrum is hard with photon number index $0 \lesssim \Gamma \lesssim +1$.

Varying the baryon loading of the flow has moderate effect in the emission in the *BATSE* energy range but profound implications in other bands. The model predicts that flows with low baryon loading (i.e. high σ_0) have powerful optical, UV and GeV emission. More on the comparison of the model with observations is presented in the next section.

5.1. Comparison with observations

The prompt GRB emission has been typically observed in the hard X-rays up to ∼1 MeV γ-rays. The spectrum in this energy range shows a characteristic sub-MeV break followed by a flat power-law γ-ray tail (e.g. Band et al. 1993). Below the break the spectrum has typical photon number index of $\Gamma \sim -1$ although much harder spectra have also been observed[2]. The observed sub-MeV break and the spectral slopes above and below the break are naturally explained by the gradual dissipation model discussed here. Furthermore, the model makes specific predictions on the prompt emission from the optical to GeV; bands that are currently (or will soon be) accessible to observations. The model predicts that the flat γ-ray tail extends up to a cutoff

[2] These hard spectra cannot be explained by the thin synchrotron model (e.g. Ghirlanda et al. 2003).

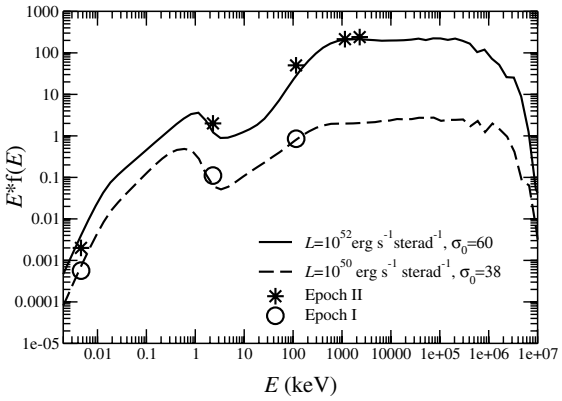

Fig. 3. Applying the model to multi frequency observations of the prompt emission of GRB 061121 (see Fig. 11 in Page et al. 2007). The circles stand for the observations of epoch I (just before the main pulse of the burst) and the stars for those of epoch II (during the pulse). Observations are blue-shifted by $1+z$ to the burst rest frame ($z = 1.131$ for GRB 061121). The solid and dashed curves show spectra for two different sets of the parameters of the flow that illustrate that the model can account for the broad-band prompt spectra.

that typically appears at ∼0.1−1 GeV. It also predicts the prompt optical and UV emission. For low baryon loading, the emission in these bands is powerful with energy flux $f(E)$ similar to that of X-rays. The optical emission is characterized by a hard spectrum. Optically bright bursts have powerful GeV emission and softer spectra below the ∼1 MeV break.

In recent years, several observations in softer bands have been made simultaneously with the prompt GRB emission. The *Swift* satellite has observed the prompt emission in the X-rays (Hill et al. 2006; Romano et al. 2006; Page et al. 2007) and ultra violet (Page et al. 2007) and robotic telescopes in the optical and infra red (e.g. Akerlof 1999; Vestrad 2005; Blake 2005; Boër et al. 2006; Vestrand et al. 2006; Klotz et al. 2006). Furthermore, *GLAST* is expected to probe the emission from GRBs up to ∼100 GeV.

Here, I compare the model to the very well sampled prompt emission of GRB 061121. This burst has been observed from optical to ∼1 MeV (Page et al. 2007). The prompt emission has been followed with XRT and UVOT on board to *Swift* and in the optical with *ROTSE* simultaneously to γ-ray observations with BAT and *Konus-Wind*. There are two time resolved spectra just before and during the main pulse of the prompt emission that appears ∼75 s after the onset of the burst. The pulse is clear in the lightcurves in all observed energy bands. The correlation between the different bands indicates that the optical, UV and X-ray and γ-ray components have common origin (i.e. they are connected to the prompt GRB). This is unlike cases where the optical lightcurves are not tracing the γ-rays (e.g. Akerlof 1999; Boër et al. 2006; Klotz et al. 2006) suggestive of a different physical origin w.r.t. that of the prompt emission.

In Fig. 3, the data shown with circles refer to the pre-spike emission (epoch I in the Page et al. 2007 terminology) and the stars to the peak observed luminosity of the burst (epoch II). The data span approximately 6 orders of magnitude in frequency from the optical to ∼1 MeV. Overplotted are the spectral predictions of the model for two different sets of parameters. The low luminosity model has $L = 10^{50}$ erg s^{-1} sterad^{-1} and $\sigma_0 = 38$ and the high luminosity one $L = 10^{52}$ erg s^{-1} sterad^{-1} and $\sigma_0 = 60$. The two models (not meant to be detailed fits) are reproducing the observations quite closely.

Note that for a given observed luminosity, the baryon loading is essentially the only free parameter of the model. This can be constrained by the ratio of the ∼1 MeV-to-optical flux. Additional constraints can come from observations of the prompt emission in harder bands. In this respect *GLAST* observations in the ∼GeV range are going to be of particular importance.

The high luminosity model (that describes the epoch II observations) is characterized by higher σ_0 with respect to the lower luminosity one. This is in qualitative agreement with the baryon loading-luminosity correlation during the evolution of the burst needed to explain observed energy-dependent properties of the GRB pulses in the context of the reconnection model (for details see Sect. 4 in GS07). However since GS07 do not consider the Thomson thin emission in the calculations, the quantitative results of Sect. 4 in GS07 have to be revisited.

6. Discussion/conclusions

The GRB emission may be result of internal collisions in a variable flow (Rees & Mészáros 1994). In the internal shock model energy is dissipated at the location of the shell collision. Particles are accelerated at the shock front to ultrarelativistic speeds and non-thermal distributions. Magnetic fields are assumed to be amplified because of plasma instabilities. The emitted spectrum depends on the distribution of the emitting particles and the strength of the shock amplified magnetic field, both of which are not understood from first principles. The emitted spectrum also depends on the properties of the flow (such as optical depth) at the radius of the collision (e.g. Pe'er et al. 2006).

As an alternative to internal shocks, magnetic dissipation in a strongly magnetized flow can power the GRB (Thompson 1994). Magnetic dissipation may lead to gradual release of energy over a wide range of radii (e.g. Drenkhahn 2002; DS02). It typically proceeds in both Thomson thick and thin regions of the flow. The released energy can be distributed to a large fraction of the particles of the flow leading to the slow heating scenario for the GRB emission (Ghisellini & Celotti 1999). The emitting particles (i.e. electrons) are heated up to mildly relativistic speeds. Because of the strong magnetic fields exchange of synchrotron photons provides an efficient mechanism for the thermalization of the electron distribution (Ghisellini et al. 1998). Since the emitting particles are thermal the resulting emission does not depend sensitively on poorly understood physics of particle acceleration in magnetic reconnection. The model is defined by just the luminosity of the flow, its baryon loading and a reconnection-rate parameter and makes direct and stable predictions for the electromagnetic spectrum.

In previous works (G06 and GS07), we calculated the photospheric emission expected from the reconnection model. The radiative transfer study was made with Monte Carlo simulations. Those calculations have shown that the flow is characterized by powerful photospheric emission with most of the energy appearing in the hard X-rays and ∼1 MeV γ-rays. This emission is the result of photons, produced deep into the flow, that are inverse Compton scattered by sub-relativistic electrons at Thomson optical depths of order of unity.

In the reconnection model, for low enough baryon-loading of the flow, there are substantial amounts of energy dissipated in its outer, Thomson thin, parts. Here I have extended the G06 calculations to include the Thomson thin emission. Energy release at large radii leads to mildly relativistic electrons that cool down though emitting synchrotron radiation and inverse Compton scattering soft photons. SSA emission dominates the observed radiation in the soft X-ray and softer bands. This soft

(e.g. optical) emission is very weak in models where dissipation is limited below or around the Thomson photosphere (see, e.g., Mészáros & Rees 2000; Pe'er et al. 2006; Ioka et al. 2007). Inverse Compton in the Thomson thin region leads to a flat high-energy spectrum that extends up to GeV energies.

The resulting spectra from the radiative transfer calculations naturally explain the observed sub-MeV break of the GRB emission and the spectral slopes above and below the break (Band et al. 1993). Furthermore, the model makes rather robust predictions for the emission in other energy bands. The flat γ-ray spectrum is expected to show a cutoff in the $\sim$0.1–1 GeV energy range that should be observable with *GLAST*. The optical and ultra violet emission can be powerful and the optical spectrum hard with photon number index $0 \lesssim \Gamma \lesssim 1$. Bright prompt optical emission is predicted to be accompanied by powerful $\sim$GeV emission and rather soft spectra below the sub-MeV break. Comparison with multi-frequency observations of the prompt emission from GRB 061121 that span from the optical to the $\sim$MeV range (Page et al. 2007) supports the model.

Acknowledgements. I thank Henk Spruit for many valuable suggestions and discussions.

References

Akerlof, C., Balsano, R., Barthelmy, S., et al. 1999, Nature, 398, 400
Band, D., Matteson, J., Ford, L., et al. 1993, ApJ, 413, 281
Blake, C. H., Bloom, J. S., Starr, D. L., et al. 2005, Nature, 435, 181
Boër, M., Atteia, J. L., Damerdji, Y., et al. 2006, ApJ, 638, L71
Coroniti, F. V. 1990, ApJ, 349, 538
Daigne, F., & Mochkovitch, R. 1998, MNRAS, 296, 275
Drenkhahn, G. 2002, A&A, 387, 714
Drenkhahn, G., & Spruit, H. C. 2002, A&A, 391, 1141 (DS02)
Ghirlanda, G., Celotti, A., & Ghisellini, G. 2003, A&A, 406, 879
Ghisellini, G., & Celotti, A. 1999, A&AS, 138, 527
Ghisellini, G., Haardt, F., & Svensson, R. 1998, MNRAS, 297, 348
Giannios, D. 2006, A&A, 457, 763 (G06)
Giannios, D., & Spruit, H. C. 2005, A&A, 430, 1
Giannios, D., & Spruit, H. C. 2006, A&A, 450, 887
Giannios, D., & Spruit, H. C. 2007, A&A, 469, 1 (GS07)
Ioka, K., Murase, K., Toma, K., Nagataki, S., & Nakamura, T. 2007, ApJ, 670, L77
Katz, J. I. 1994, ApJ, 432, L107
Kirk, J. G., & Skjæraasen, O. 2003, ApJ, 591, 366
Klotz, A., Gendre, B., Stratta, G., et al. 2006, A&A, 451, L39
Kobayashi, S., Piran, T., & Sari, R. 1997, ApJ, 490, 92
Lyubarsky, Y. E. 2005, MNRAS, 358, 113
Lyubarsky, Y., & Kirk, J. G. 2001, ApJ, 547, 437
Lyutikov, M., & Blandford, R. 2003 [arXiv:astro-ph/0312347]
Mahadevan, R., Narayan, R., & Yi, I. 1996, ApJ, 465, 327
Mészáros, P., & Rees, M. J. 2000, ApJ, 530, 292
Mimica, P., Aloy, M. A., Müller, E., & Brinkmann, W. 2005, A&A, 441, 103
Nakar, E., & Piran, T. 2002, ApJ, 572, L139
Paczynski, B., & Xu, G. 1994, ApJ, 427, 708
Page, K. L., Willingale, R., Osborne, J. P., et al. 2007, ApJ, 663, 1125
Pe'er, A., Mészáros, P., & Rees, M. J. 2006, ApJ, 642, 995
Petrosian, V. 1981, ApJ, 251, 727
Preece, R. D., Briggs, M. S., Mallozzi, R. S., et al. 1998, ApJ, 506, L23
Rees, M. J., & Mészáros, P. 1994, ApJ, 430, L93
Spruit, H. C., Daigne, F., & Drenkhahn, G. 2001, A&A, 369, 694
Stern, B. 1999, in High Energy Processes in Accreting Black Holes, ed. J. Poutanen, & R. Svensson (San Francisco: ASP), ASP Conf. Ser., 161, 277
Stern, B. E., & Poutanen, J. 2004, MNRAS, 352, L35
Tavani, M. 1996, ApJ, 466, 768
Thompson, C. 1994, MNRAS, 270, 480
Thompson, C. 2006, ApJ, 651, 333
Vestrand, W. T., Wozniak, P. R., Wren, J. A., et al. 2005, Nature, 435, 178
Vestrand, W. T., Wren, J. A., Wozniak, P. R., et al. 2006, Nature, 442, 172
Wardziński, G., & Zdziarski, A. A. 2000, MNRAS, 314, 183
Zdziarski, A. A., Poutanen, J., Mikolajewska, J., et al. 1998, MNRAS, 301, 435